

# Efficient generation of third harmonics in Yb-doped femtosecond fiber laser via spatial and temporal walk-off compensation

Meng Zhang (张萌)<sup>1</sup>, Yuxi Chu (储玉喜)<sup>1\*</sup>, Jun Zhao (赵君)<sup>1</sup>, Dongyu Yan (闫东钰)<sup>1</sup>, Yongzhi Li (李永智)<sup>1</sup>, Genu Bi (毕根毓)<sup>1</sup>, Bowen Liu (刘博文)<sup>1</sup>, and Minglie Hu (胡明列)<sup>1,2</sup>

<sup>1</sup>Ultrafast Laser Laboratory, Key Laboratory of Opto-electronic Information Science and Technology of Ministry of Education, School of Precision Instruments and Opto-electronics Engineering, Tianjin University, Tianjin 300072, China

<sup>2</sup>E-mail: huminglie@tju.edu.cn

\*Corresponding author: [chuyuxi@tju.edu.cn](mailto:chuyuxi@tju.edu.cn)

Received January 4, 2021 | Accepted January 12, 2021 | Posted Online February 3, 2021

On the basis of a home-made femtosecond Yb-doped fiber laser, we designed a compact and efficient third harmonic generation scheme by a simple compensation plate of  $\beta$ -BaB<sub>2</sub>O<sub>4</sub> crystal. The compensation plate is optimized through its thickness and cutting angle to reverse both spatial and temporal walk-off. By optimizing the parameters of the compensation plate and incident light intensity, a maximum output of 2.23 W with a repetition rate of 1 MHz at 345 nm is obtained, which implies a conversion efficiency of 23% from the infrared to ultraviolet.

**Keywords:** ultrafast nonlinear optics; harmonic generation and mixing; ultraviolet; compensation plates.

**DOI:** [10.3788/COL202119.031402](https://doi.org/10.3788/COL202119.031402)

## 1. Introduction

The development of high-repetition-rate ultra-short laser sources providing extremely intense pulses, especially in the ultraviolet (UV) region, is of great importance in microscopy, ultrafast spectroscopy, quantum optics, and scientific research<sup>[1-3]</sup>. The short wavelength with high single-photon energy allows rapid absorption and a small focal spot, potentially enabling high machining accuracy and patterning ability even in wide bandgap materials<sup>[4]</sup>.

In recent times, extensive research has been conducted on nonlinear frequency up-conversion of picosecond lasers generating high-power UV<sup>[5,6]</sup> and blue light<sup>[7,8]</sup> through third harmonic generation (THG) and second harmonic generation (SHG), respectively. Compared with picosecond lasers, femtosecond lasers have much narrower pulse duration and higher peak intensity and can be powerful tools in laser precision machining<sup>[9,10]</sup>. Recently, there have been several reports on the development of femtosecond UV laser sources based on nonlinear frequency conversion in femtosecond IR lasers<sup>[11-14]</sup>. However, the temporal walk-off effect caused by group velocity mismatch will reduce the overlap of three interacting waves in the sum-frequency generation (SFG) crystal, decreasing conversion efficiency. Traditionally, a delay line is used to control the temporal overlap after the unconverted pump, and second harmonic (SH) beams are separated using a dichroic mirror<sup>[15,16]</sup>.

In this way, the THG results of up to 22% near-IR-to-UV conversion efficiency are obtained based on an Yb fiber laser with 5 W average power at 260 fs pulses<sup>[15]</sup>. The most common drawbacks of such a delay line system lay with their bulky size and complicated system design. Besides, the delay line containing separated and recombined beams is difficult to align and sensitive to minor disturbances in the environment.

Alternatively, introducing one or multiple compensation plates (CPs) with relative anomalous dispersion enables tabletop UV laser systems with simple series configuration and high conversion efficiency. The potential of CPs can be seen by the impressive 800 to 270 nm THG efficiencies of 5.3%<sup>[17]</sup> and 8.48%<sup>[18]</sup> with Ti:sapphire laser systems. However, the repetition rates of high-energy femtosecond Ti:sapphire lasers are limited to a few kilohertz, which is not suitable for material processing applications<sup>[19-21]</sup>. In addition, the bulky design and high price make them less competitive compared with fiber lasers. In particular, the rapid development of Yb-doped femtosecond fiber lasers has brought about a new generation of high-power, compact, stable, and cost-effective laser sources for scientific research and industrial applications<sup>[22-24]</sup>. However, to the best of our knowledge, there are no studies to date on compact and practical UV lasers based on femtosecond fiber lasers with CPs.

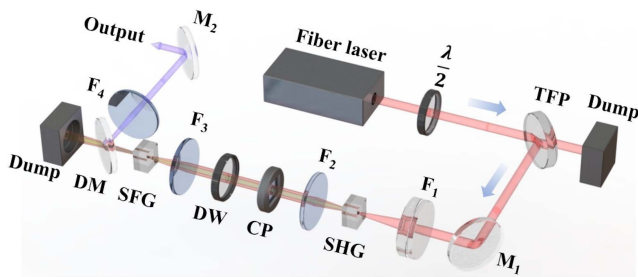
In this article, we present a cascaded THG scheme with a CP of  $\beta$ -BaB<sub>2</sub>O<sub>4</sub> (BBO) crystal based on a home-made Yb-doped

femtosecond fiber laser. The thickness and cutting angle of the CP are optimized to reverse both the spatial and temporal walk-off. By optimizing the parameters of the CP and incident light intensity, the efficient generation of UV output is achieved with a power as high as 2.23 W and a near-IR-to-UV conversion efficiency of  $\sim 23\%$ . To the best of our knowledge, this is the first experimental report on a UV source at 345 nm based on an Yb-doped femtosecond fiber laser with the CP providing output power  $> 2$  W at 1 MHz. The tabletop UV source has a power stability of 0.67% RMS and almost no power degradation over 6 h. By contrast, the maximum UV output power with the complex traditional delay line is 1.9 W due to the loss of two dichroic mirrors and multiple reflections, and the power stability is 1.32% RMS with a clear drift at a rate of approximately 0.73% per hour.

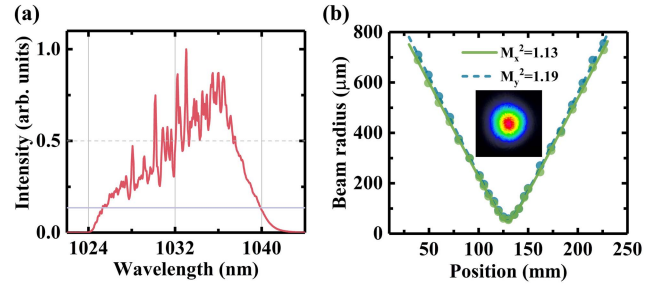
## 2. Experimental Setup

Figure 1 illustrates a schematic diagram of the experimental arrangement. The system employed a home-made Yb-doped femtosecond fiber laser based on the chirped-pulse amplification technique, producing maximum output pulse energy of  $10 \mu\text{J}$ . The laser can be operated from 100 kHz to 1 MHz through an acousto-optic modulator, which implies that the maximum average power is 10 W at a 1 MHz repetition rate. Figure 2(a) shows a spectral width of 14.6 nm ( $1/e^2$ ) centered at 1032.6 nm. The pulse width is approximately 420 fs. Figure 2(b) shows the  $M^2$  factors ( $M^2 < 1.2$ ), and the inset shows the near-field beam profile of the pump laser. The optimization of THG was performed at a 1 MHz operational frequency.

The input power to the nonlinear crystals was controlled using a half-wave plate ( $\lambda/2$ ) and a thin-film polarizer (TFP). The maximum pump power incident onto the SHG crystal was 9.7 W after reflections of the TFP and plano mirror. A 3 mm long and  $5 \text{ mm} \times 5 \text{ mm}$  aperture  $\text{LiB}_3\text{O}_5$  (LBO) crystal cut at  $\theta = 90^\circ$  and  $\varphi = 13.2^\circ$  in the optical  $x$ - $y$  plane for critical phase matching was chosen as the SHG crystal to match industrial applications. The pump beam was focused at the center of the SHG crystal using an achromatic lens,  $F_1$ , with a focal length  $f_1 = 200 \text{ mm}$  when a trade-off between the conversion efficiency



**Fig. 1.** Experimental setup.  $\lambda/2$ , half-wave plate; TFP, thin-film polarizer;  $M_1$ , plano mirror at 1030 nm;  $F_1 - F_4$ , lenses; SHG, 3 mm LBO crystal; CP, compensation plate; DW, dual-wavelength waveplate; SFG, 3 mm BBO crystal; DM, dichroic mirror;  $M_2$ , plano mirror at 345 nm.



**Fig. 2.** (a) Spectrum and (b)  $M^2$  factors of Yb-doped femtosecond fiber laser; the inset in (b) is the near-field beam profile.

and damage threshold of the SHG crystal was considered. The achromatic lens was optimized to minimize the chromatic aberration across a broad bandwidth, and then the high beam quality of the SH beam was obtained. The measured beam waist diameter of the fundamental beam is  $\sim 112 \mu\text{m}$ . We achieve a maximum SHG conversion efficiency of 42% corresponding to 4.1 W average power at 517 nm in the LBO, as shown in Fig. 3(a). The inset in Fig. 3(a) shows the SH beam profile at the maximum average output power, and the measured ellipticity value is  $\omega_{\text{minor}}/\omega_{\text{major}} = 0.93$ . Figure 3(b) shows the measured spectrum of the SH beam with a spectral bandwidth of 5.5 nm ( $1/e^2$ ). The measured beam quality factors are  $M_x^2 = 1.48$  and  $M_y^2 = 1.44$  [Figs. 3(c) and 3(d)].

For the SFG of the unconverted pump and the SH beam into UV radiation at 345 nm, we used a 3 mm long and a  $4 \text{ mm} \times 4 \text{ mm}$  aperture BBO crystal cut at  $\theta = 32.1^\circ$  for type I ( $o + o \rightarrow e$ ) critical phase matching due to its high effective nonlinear coefficient  $d_{\text{eff}}$  ( $d_{\text{eff}} = 2.01 \text{ pm/V}$ , SNLO software package) value. To ensure the phase matching of type I, a dual-wavelength waveplate (DW) was used to rotate the polarization of the

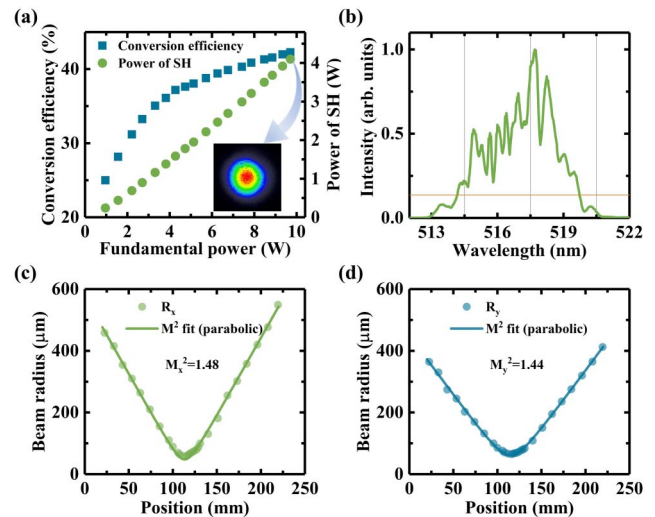


**Fig. 3.** (a) Average output power and conversion efficiency of the SH beam as functions of the fundamental power. Inset, the near-field beam profile of the SH beam at maximum average power output. (b) Spectrum, (c)  $M_x^2$ , and (d)  $M_y^2$  factors of the SH beam.

fundamental light individually to coincide with the polarization of the SH beam. The collimation ( $F_2$ ) and focusing ( $F_3$ ) lenses were placed in front of the BBO crystal to achieve optimum generation conditions, which satisfied the  $4f$  condition to minimize the aberration. To efficiently produce UV light, a CP was used to reverse both the spatial and temporal walk-off between the pump and SH pulse after SHG.

### 3. Design of the CP

As shown in Fig. 4(a), the CP can be used to reverse both the spatial and temporal walk-off due to its birefringence effect. To obtain a good compensation effect, each component's spatial and temporal walk-off should be theoretically calculated. First, the walk-off angle of LBO is 8.0 mrad, and the walk-off distance is  $\Delta d = 3 \times 8.0 = 24 \mu\text{m}$ . There is no spatial walk-off between the pump and the SH beams in the type I SFG crystal. Second, the theoretical delay time induced by each component between the central wavelengths of the fundamental and the SH beams is given in Table 1<sup>[25]</sup>. The focal lengths of  $F_2$  and  $F_3$  were both 100 mm. Hence, to control the spatial and temporal

overlap, the CP was designed to compensate for the spatial deviation of the SH beam ( $\Delta d = 24 \mu\text{m}$ ) and the delay time before the BBO crystal. Traditionally, the CP is a birefringent crystal that is cut with an appropriate length and angle, such as BBO and calcite<sup>[26]</sup>. We chose BBO here because of its higher damage threshold and better surface quality. Figure 4(b) shows the group refractive index of SH (blue curves) and fundamental (red curves) beams as a function of cutting angle  $\theta$  in the optical  $x-z$  plane of BBO. When the SH and fundamental beams are e and o waves, respectively, the SH pulses transmit faster than the fundamental beam in the BBO plate designed at a certain angle greater than  $38.37^\circ$  (purple-shaded region). The temporal and spatial compensation of a 1-mm-thick BBO crystal with different cutting angles  $\theta$  is illustrated in Fig. 4(c). Hence, by optimizing the thickness  $L$  and cutting angle  $\theta$ , the CP can compensate for the required space and time delay.

### 4. Results and Discussion

To obtain optimum SFG efficiency, we used CPs with different compensation capabilities (Table 2). Each CP is distinguished for different delay times because the temporal walk-off dominates before SFG. Then, the UV output power for different CPs with  $f_2 = 100 \text{ mm}$  was measured at the maximum pump power, as shown in Fig. 5(a). Different focusing lenses ( $F_3$ ) were used to optimize the incident light intensity inside the BBO for maximizing the output UV power. Three lenses with focal lengths of 100, 125, and 150 mm were tested. Obviously, the output UV power is the highest using  $f_3 = 100 \text{ mm}$ . The lens system with  $f_2 = f_3 = 100 \text{ mm}$  is 1:1, resulting in pump and SH beam waist diameters of  $\sim 112 \mu\text{m}$  and  $97 \mu\text{m}$ , respectively. If not compensated, that is  $\Delta t = 0$ , the measured UV output power is 1.25 W. The output powers at 345 nm,  $P_{UV}$ , of CP1 and CP2 are 1.9 and 2.1 W, respectively. The UV output power increases with  $\Delta t$  until the maximum output power is obtained using CP3. Subsequently, the output power of the UV pulses begins to decline due to overcompensation. Figure 5(b) shows the average output power and conversion efficiency for CP3 as functions of pump power. The UV power and UV efficiency increase with the increase of the pump power, resulting in a maximum UV power of 2.23 W, corresponding to a single-pass near-IR-to-UV conversion efficiency as high as 23%. The inset in Fig. 5(b) shows the UV beam profile whose measured ellipticity value is 0.78

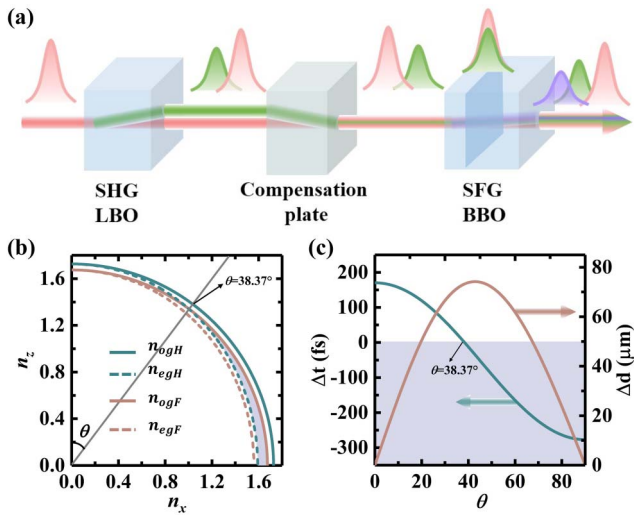


**Fig. 4.** (a) Spatial and temporal walk-off effects and their optimization using a CP. Red, fundamental pulses; green, SH pulses; violet, UV pulses. (b) Group refractive index curves of SH (blue curves) and fundamental (red curves) beams including o (solid line) and e (dashed line) waves in the optical  $x-z$  plane of BBO. (c) Delay time and walk-off distance of a 1-mm-thick BBO crystal as functions of  $\theta$ . Negative value of  $\Delta t$  means that the fundamental pulses lag behind the SH pulses.

**Table 1.** Delay Time between Green and Pump Beams.

	LBO	$F_2$	$F_3$	DW	BBO
$\Delta t$ (fs)	160	223.5	223.5	75.5	520

**Table 2.** Key Parameters of CPs.

No.	1	2	3	4	5 (1 + 2)	
$L$ (mm)	1.65	2	2.6	3	1.65	2
$\theta$	$83.3^\circ$	$80^\circ$	$85^\circ$	$83^\circ$	$83.3^\circ$	$80^\circ$
$\Delta t$ (fs)	-420	-527	-712	-811	-947	
$ \Delta d $ ( $\mu\text{m}$ )	24	47	31	49	23	

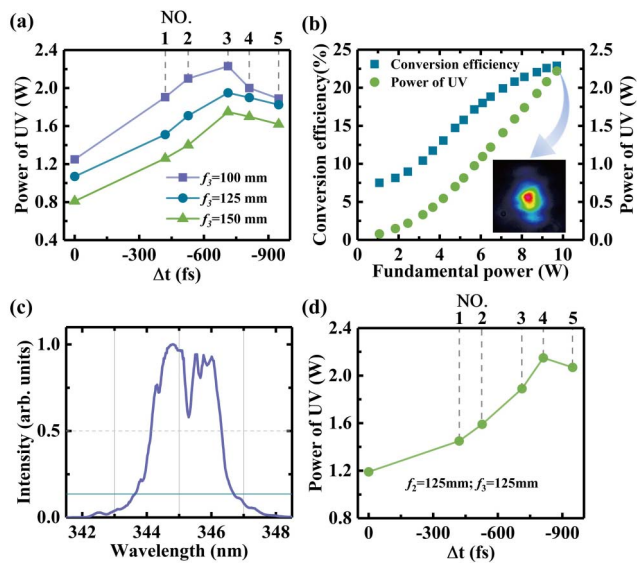


**Fig. 5.** Experimental results of SFG. (a) UV output power for different CPs with different focusing lenses. (b) UV output power and conversion efficiency as functions of the fundamental power. Inset, near-field beam profile of the UV beam at maximum average output power. (c) UV spectrum at maximum average output power. (d) UV output power for different CPs with  $f_2 = f_3 = 125$  mm.

at maximum average output power, and Fig. 5(c) shows its corresponding spectrum. To further investigate the effect of these CPs, we measured the UV power for different temporal walk-off induced by different lenses, as shown in Fig. 5(d). The system of  $f_2 = f_3 = 125$  mm has the same spot size in the BBO as  $f_2 = f_3 = 100$  mm. The center thicknesses of the  $f = 100$  mm and  $f = 125$  mm focal length lenses are 2.2 and 3.3 mm with 223.5 and 335.3 fs delay times, respectively. A maximum UV power output of 2.15 W was achieved by the system of  $f_2 = f_3 = 125$  mm using CP4. Despite the temporal walk-off of the system being different, high output UV power can still be obtained with the CP.

By contrast, we reproduced the experiment by using the conventional delay line with  $f_2 = f_3 = 100$  mm. Ideally, the tunable delay line could provide a continuously variable delay time, and thus higher UV output power could be achieved. Unfortunately, the maximum UV output power (efficiency) is 1.9 W (19.6%) due to the loss of two dichroic mirrors and multiple reflections. Figure 6(a) shows the output power at 345 nm and conversion efficiency as functions of pump power. The inset in Fig. 6(a) shows the UV beam profile at the maximum average output power, and the measured ellipticity value is 0.84. The elliptic UV beam profile can be attributed to the spatial walk-off of the beam and thermal distortion caused by two-photon absorption in the BBO crystal. Finally, we measured the power stability of the UV source. The tabletop UV laser system was operated for 6 h in an open environment. As Fig. 6(b) shows, there is almost no power degradation over 6 h by the CP method. The periodic fluctuation of the UV output power may be due to the periodic change of the ambient temperature because the measurement

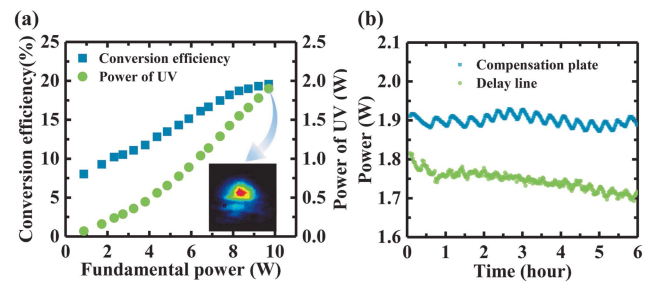


**Fig. 6.** (a) UV output power and conversion efficiency as functions of the fundamental power using the conventional delay line. Inset, near-field beam profile of the UV beam at maximum average output power. (b) Power stability tests of the CP and conventional delay line, respectively, for 6 h.

was done without any temperature control. The power stability is 0.67% RMS and 3% peak-to-peak power fluctuation. By comparison, the delay line's power stability is 1.32% RMS and 7% peak-to-peak power fluctuation, with a clear drift at a rate of approximately 0.73% per hour. The decrease in power stability compared with the CP case can be attributed to complicated system design containing separated and recombined beams.

## 5. Conclusions

In conclusion, we have designed a compact and efficient THG scheme with a simple CP of BBO crystal based on a femtosecond Yb fiber laser source. The thickness and cutting angle of the CP are optimized to reverse both the spatial and temporal walk-off. By optimizing the parameters of the CP and incident light intensity, a maximum UV output of 2.23 W is obtained at a repetition rate of 1 MHz when the compensation time induced by the CP is  $-712$  fs, corresponding to a single-pass near-IR-to-UV conversion efficiency as high as 23%. The tabletop UV laser system has a power stability of 0.67% RMS in 6 h with almost no power degradation. By contrast, the maximum UV output power with the complex traditional delay line is 1.9 W due to the loss of two dichroic mirrors and multiple reflections, and the power stability is 1.32% RMS with a clear drift at a rate of approximately 0.73% per hour. In the future, even more compact THG structures based on the CP method without collimation and focusing lenses can be expected from hundreds of microjoules ( $\mu$ J) pulse energy IR driving lasers. The method shows remarkable potential for applications in stable, compact, and efficient UV generation.

## Acknowledgement

This work was supported by the National Natural Science Foundation of China (NSFC) (Nos. 61805174 and U1730115), Natural Science Foundation of Tianjin (No. 20JCQNJC01180), and Research and Development Program in Key Areas of Guangdong Province, China (No. 2020B090922004).

## References

1. T. A. Klar and S. W. Hell, "Subdiffraction resolution in far-field fluorescence microscopy," *Opt. Lett.* **24**, 954 (1999).
2. M. Bauer, "Femtosecond ultraviolet photoelectron spectroscopy of ultra-fast surface processes," *J. Phys. D* **38**, R253 (2005).
3. J. Yin, J. Ren, H. Lu, Y. Cao, H. Yong, Y. Wu, C. Liu, S. Liao, F. Zhou, Y. Jiang, X. Cai, P. Xu, G. Pan, J. Jia, Y. Huang, H. Yin, J. Wang, Y. Chen, C. Peng, and J. Pan, "Quantum teleportation and entanglement distribution over 100-kilometre free-space channels," *Nature* **488**, 185 (2012).
4. S. Gao, Z. Li, Z. Hu, F. Yu, Q. Chen, Z. Tian, and H. Sun, "Diamond optical vortex generator processed by ultraviolet femtosecond laser," *Opt. Lett.* **45**, 2684 (2020).
5. W. Chen, B. Liu, Y. Song, L. Chai, Q. Cui, Q. Liu, C. Wang, and M. Hu, "High pulse energy fiber/solid-slab hybrid picosecond pulse system for material processing on polycrystalline diamonds," *High Power Laser Sci. Eng.* **6**, e18 (2018).
6. P. Zhu, D. Li, Q. Liu, J. Chen, S. Fu, P. Shi, K. Du, and P. Loosen, "39.1  $\mu$ J picosecond ultraviolet pulses at 355 nm with 1 MHz repeat rate," *Opt. Lett.* **38**, 4716 (2013).
7. R. Bhandari and T. Taira, "> 6 MW peak power at 532 nm from passively Q-switched Nd:YAG/Cr<sup>4+</sup>:YAG microchip laser," *Opt. Express* **19**, 19135 (2011).
8. N. Ma, M. Chen, C. Yang, S. Lu, X. Zhang, and X. Du, "High-efficiency 50 W burst-mode hundred picosecond green laser," *High Power Laser Sci. Eng.* **8**, e1 (2020).
9. X. Fu, Z. Chen, D. Han, Y. Zhang, H. Xia, and H. Sun, "Laser fabrication of graphene-based supercapacitors," *Photon. Res.* **8**, 577 (2020).
10. D. Yan, B. Liu, Y. Chu, H. Song, L. Chai, M. Hu, and C. Wang, "Hybrid femtosecond laser system based on a Yb:KGW regenerative amplifier for NP polarization," *Chin. Opt. Lett.* **17**, 041404 (2019).
11. J. Rothhardt, C. Rothhardt, M. Müller, A. Klenke, M. Kienel, S. Demmler, T. Elsmann, M. Rothhardt, J. Limpert, and A. Tünnermann, "100 W average power femtosecond laser at 343 nm," *Opt. Lett.* **41**, 1885 (2016).
12. H. Ye, L. Pontagnier, C. Dixneuf, G. Santarelli, and E. Cormier, "Multi-GHz repetition rate, femtosecond deep ultraviolet source in burst mode derived from an electro-optic comb," *Opt. Express* **28**, 37209 (2020).
13. A. Rao, N. Chaitanya, and G. Samanta, "High-power, high repetition-rate, ultrafast fibre laser based source of DUV radiation at 266 nm," *OSA Continuum* **2**, 99 (2018).
14. M. Müller, A. Klenke, T. Gottschall, R. Klas, C. Rothhardt, S. Demmler, J. Rothhardt, J. Limpert, and A. Tünnermann, "High-average-power femtosecond laser at 258 nm," *Opt. Lett.* **42**, 2826 (2017).
15. N. Apurv Chaitanya, A. Aadhi, M. Jabir, and G. Samanta, "High-power, high-repetition-rate, Yb-fiber laser based femtosecond source at 355 nm," *Opt. Lett.* **40**, 4269 (2015).
16. H. Liu, M. Hu, B. Liu, Y. Song, L. Chai, A. Zheltikov, and C. Wang, "Compact high-power multiwavelength photonic-crystal-fiber-based laser source of femtosecond pulses in the infrared-visible-ultraviolet range," *J. Opt. Soc. Am. B* **27**, 2284 (2010).
17. Y.-L. Wang, X.-G. Zhou, H. Wu, and L.-E. Ding, "Efficient collinear frequency tripling of femtosecond laser with compensation of group velocity delay," *Chin. Phys. B* **18**, 4308 (2009).
18. H. Meng, H. Liu, J. Huang, H. Wu, J. Deng, S. Dai, W. Weng, and W. Lin, "Generation of tunable ultrafast ultraviolet third harmonic by collinear compensation of group-velocity mismatch," *Opt. Commun.* **353**, 96 (2015).
19. D. Spence, P. Kean, and W. Sibbett, "60-fsec pulse generation from a self-mode-locked Ti:sapphire laser," *Opt. Lett.* **16**, 42 (1991).
20. Y. Nabekawa, Y. Kuramoto, T. Togashi, T. Sekikawa, and S. Watanabe, "Generation of 0.66-TW pulses at 1 kHz by a Ti:sapphire laser," *Opt. Lett.* **23**, 1384 (1998).
21. H. Liu, G. Wang, J. Jiang, W. Tian, D. Zhang, H. Han, S. Fang, J. Zhu, and Z. Wei, "Sub-10-fs pulse generation from a blue laser-diode-pumped Ti:sapphire oscillator," *Chin. Opt. Lett.* **18**, 071402 (2020).
22. M. Fermann and I. Hartl, "Ultrafast fibre lasers," *Nat. Photon.* **7**, 868 (2013).
23. T. Eidam, J. Rothhardt, F. Stutzki, F. Jansen, S. Hädrich, H. Carstens, C. Jauregui, J. Limpert, and A. Tünnermann, "Fiber chirped-pulse amplification system emitting 38 GW peak power," *Opt. Express* **19**, 255 (2010).
24. P. Wan, L. Yang, and J. Liu, "All fiber-based Yb-doped high energy, high power femtosecond fiber lasers," *Opt. Express* **21**, 29854 (2013).
25. A. Smith, D. Armstrong, and W. Alford, "Increased acceptance bandwidths in optical frequency conversion by use of multiple walk-off-compensating nonlinear crystals," *J. Opt. Soc. Am. B* **15**, 122 (1998).
26. G. Ghosh, "Dispersion-equation coefficients for the refractive index and birefringence of calcite and quartz crystals," *Opt. Commun.* **163**, 95 (1999).